Novel Long-Term Immobilization Method for Radioactive Iodine-129 Using a Zeolite/Apatite Composite Sintered Body

Yujiro Watanabe,*,† Toshiyuki Ikoma,‡ Hirohisa Yamada,§ Yasushi Suetsugu,‡ Yu Komatsu,† Geoffrey W. Stevens,|| Yusuke Moriyoshi,⊥ and Junzo Tanaka#

Advanced Materials Science Research & Development Center, Environmental Research Institute, Kanazawa Institute of Technology, 3-1 Yatsukaho, Hakusan, Ishikawa 924-0838, Japan, Biomaterials Center, National Institute for Materials Science, 1-2-1 Sengen, Tsukuba, Ibaraki 305-0047, Japan, Photocatalystic Materials Center, National Institute for Materials Science, 1-1 Namiki, Tsukuba, Ibaraki 305-0044, Japan, Department of Chemical & Biomolecular Engineering, The University of Melbourne, Melbourne, Victoria 3010, Australia, Faculty of Engineering, Hosei University, 3-7-2 Kajinocho, Koganei, Tokyo 184-8584, Japan, and Department of Metallurgy and Ceramics Science, Tokyo Institute of Technology, 2-12-1, S7-5 Ookayama, Meguro, Tokyo 152-8550, Japan

ABSTRACT The amount of radioactive iodine generated from nuclear power plants is expected to increase with the proliferation of nuclear energy production, and long-term immobilization methods for such radioactive elements need to be developed to make nuclear energy sustainable. The standard immobilization method of radioactive elements, vitrification, is not very effective for radioactive iodine-129 because of the low solubility of iodine in silicate melts, its very high volatility at standard vitrification process temperatures, and its instability in the alkaline environment of deep geological layers below 300 m. We have developed a novel three-phase ceramic composite produced by a sintering process. Iodine adsorbed onto Ca-type zeolite A was covered with a hydroxyapatite nanolayer through the exchange reaction of ammonium with calcium. Clusters of iodine of 30 nm within the zeolite structure were found to be thermally stable up to 1253 K because of the partial blockage of the α-cage apertures by ammonium ions and the partial change from a crystalline phase to an amorphous phase at 473 K. No gasification of iodine molecules was found to occur during the sintering process. The outer phase was highly crystalline hydroxyfluorapatite in which the hydroxyapatite nanolayer plays an important role for successful sintering. The elution of iodine in low-dioxygen water, similar to that found within the Earth's crust, was investigated and was found to occur only in the surface layer of the sintered body.

KEYWORDS: apatite • zeolites • iodine • nanostructure • encapsulation

INTRODUCTION

Nuclear power plants for energy production have been constructed for the past 53 years. Recently, there has been a resurgence of interest in nuclear power because of its low carbon output. Global warming, attributed to greenhouse gas emission, is becoming an urgent problem not only for humans but also for the entire biosphere. Nuclear power generation is one method of producing sustainable energy without excessive greenhouse gas emission. However, radioactive wastes produced at every stage of the nuclear fuel cycle must be safely managed. In particular, radioactive iodine-129, caused by the fission of uranium atoms, has a long half-life of 15.7×10^6 years. The concentration of this isotope in high-level radioactive waste from reprocessing plants is 0.2 wt % (1). Standard immobilization methods, such as vitrification, are not very effective for the long-term storage of iodine-129 because of the low solubility of iodine in silicate melts, its very high volatility at standard vitrification process temperatures (2), and its instability in the alkaline environment of deep geological layers below 300 m. Thus, the development of effective immobilization methods and suitable storage materials is of great importance for future nuclear energy options. Iodine-129 can be successfully collected by adsorbents with high specific surface areas, such as silver-impregnated hydrophobic materials (3, 4) and silver-impregnated alumina with a double-pore structure (5). These adsorbents have been investigated with regard to the reactivity of silver with iodine and improvement of their thermally stability. The borosilicate glasses, cupric/calcium/phosphate compounds, imogolite, clay, and lignite coal are also candidates for stable immobilization materials for iodine (2, 6−8).

Zeolites are unique ecomaterials with high specific surface areas and ion-exchange abilities (9, 10) and possess a nanoporous structure. Harmful cations and molecules can be absorbed through channels and cages in these materials (9−13). The Linde type-A zeolite, zeolite A, is one of the most

* Corresponding author. Tel: +81 76 274 9277. Fax: +81 76 274 9251. E-mail: yujiro@neptune.kanazawa-it.ac.jp.
Received for review April 10, 2009 and accepted June 11, 2009
† Kanazawa Institute of Technology.
‡ Biomaterials Center, National Institute for Materials Science.
§ Photocatalystic Materials Center, National Institute for Materials Science.
|| The University of Melbourne.
⊥ Hosei University.
Tokyo Institute of Technology.
DOI: 10.1021/am900251m

well-known synthetic zeolites. It has the structure $(X_{12/m})$-$(Si_{12}Al_{12}O_{48}) \cdot 27H_2O$, where X is a cation and m is the charge number, with α and β cages, of which the free diameters are 1.14 and 0.66 nm, and has the highest cation-exchange capacity of any zeolite. The aluminosilicate framework has two types of polyhedra; one is a simple cubic arrangement of eight tetrahedra (double 4-rings), and the other is a truncated octahedron of 24 tetrahedra (β cages) interconnected by $(Si, Al)_6O_6$ rings with 0.22 nm free apertures. The center of the unit cell is a large cavity (α cage) interconnected by $(Si, Al)_8O_8$ rings with 0.42 nm free apertures (10). An iodine molecule (I_2) is 0.40 nm in diameter and can pass through and adsorb into zeolites with free apertures larger than 0.40 nm, such as X-type zeolites with a free aperture of 0.74 nm, clinoptilolite-type zeolites with a free aperture of 0.72 nm, and zeolite A with a free aperture of 0.42 nm (1, 10, 13−18). However, iodine elimination from the cages can easily occur during heat treatment at relatively low temperatures because the apertures are open. It is thus necessary to be able to close the apertures in some way. The control of apertures by cations such as sodium, potassium, ammonium, and calcium has been reported by many researchers (10, 18). The conversion of synthetic zeolites to an amorphous structure by heat and pressure has received considerable attention as a potential technique for glass production in recent years (19−22). In particular, NH_4-zeolite A is easily converted into an amorphous structure at low temperature (473 K) (21). These methods may be useful as barriers to the elimination of iodine from zeolite A.

Hydroxyapatite $[Ca_{10}(PO_4)_6(OH)_2$ (HA)] and hydroxyfluorapatite $[Ca_{10}(PO_4)_6(OH/F)_2$ (HFA)] (23−29) have low-solubility products of less than 5.4×10^{-119} (K_{sp}; $mol^{18}\ L^{-18}$) and exhibit particularly high stability in an alkaline solution (30). Sintering methods for HA and HFA dense bodies have been widely investigated (31−37) and include conventional methods (31, 32), a post-sintering process (33), pulse electric current sintering (PECS) (34−36), and pressureless sintering under oxygen and argon atmospheres (37, 38). Among these, the PECS method had been shown to produce a sintered body with a relative density of 100% at low temperature and in a shorter duration because of the rapid heating rate. The low solubilities of dense HA and HFA are advantageous for long-term radioisotope immobilization by solidification. However, their adsorption ability and thermal stability with iodine need to be improved.

Although sintered iodine-adsorbed Ca-type zeolite A (I_2-zeolite A)/HFA is a promising material for radioactive immobilization, its reliability is quite low because of breakage and cracking that occur during the sintering process. This is caused by a mismatch of the thermal expansion coefficients of the components. To improve the reliability of the material during sintering, the synthesis of a buffer nanolayer of HA on the zeolite is very important.

Here we introduce a novel encapsulation method for the long-term immobilization of radioactive iodine, in which the iodine is absorbed into Ca-type zeolite A ($Ca_{5.72}Na_{0.56}Si_{12}Al_{12}$-$O_{48}$: Ca-zeolite A), whose surface is covered with a HA nanolayer to prevent breakage or cracking during the sintering process and the outer phase is surrounded with HFA. We investigated the stability of iodine molecules in the zeolite structure and the elution of iodine from the sintered composite. The effectiveness of zeolite nanoarchitechnology for radioactive immobilization is also discussed.

EXPERIMENTAL SECTION

Materials Preparation. Ca-type zeolite A (Ca-zeolite A) was synthesized from Na-zeolite A (Wako Pure Chemicals Industries, Ltd., Osaka, Japan) by the method reported previously (35, 37, 39), and the chemical composition was determined by inductively coupled plasma atomic emission spectroscopy (ICP-AES; Seiko HVR 1700, Tokyo, Japan). Iodine was adsorbed in Ca-zeolite A sieved using a No. 200 sieve. A total of 5.0 g of Ca-zeolite A was dried at 723 K for 24 h and placed in a silica tube of 15 mm in diameter and 15 cm in length. Silica wool was used as a stopper at the top and bottom of the tube. The top part of the tube was kept at 373 K by a mantle heater and the bottom at 298 K. A total of 3.0 g of nonradioactive iodine (^{127}I; Wako Pure Chemicals Industries, Ltd., Osaka, Japan) was passed through the tube using a He carrier gas at a flow rate of 100 cm^3/min. The iodine-containing gas was in contact with the sample for 72 h.

I_2-zeolite A was used for the HA coating. A total of 2.0 g of I_2-zeolite A was immersed in 200 mL of a 1 M $(NH_4)_3PO_4$ solution at pH 9.5 in a sealed Teflon bottle (500 mL). The suspension was then heated at 353 K for 8 h (37). The resultant samples were filtered with a 0.45-μm membrane filter, rinsed with 500 mL of distilled water three times to remove excess cations, and subsequently dried at 373 K for 24 h. The crystal phases were characterized by X-ray diffraction (XRD; Rigaku Rint2200, Tokyo, Japan) analysis after heat treatment at various temperatures. Morphology and elemental analysis were carried out using scanning electron microscopy (SEM; Hitachi S5200, Tokyo, Japan), scanning transmission electron microscopy (STEM; Hitachi HD2000, Tokyo, Japan), and energy-dispersive X-ray spectrometry (EDX; EDAX Genesis 4000, Mahwah, NJ). The samples, dispersed into distilled water using ultrasonic agitation, were mounted and dried on a Cu grid.

The iodine in the sample was qualified by ion chromatography (IC; Waters 2690, Tokyo, Japan). The solutions for IC were prepared as follows. The samples were mixed with Na_2CO_3 in a platinum crucible and slowly heated using a gas burner, and the mixtures were dissolved in a hydrochloric acid solution. The thermal stability of the iodine was investigated by thermogravimetry−differential thermal analysis/mass spectrometry (TG−DTA/MS; Rigaku Thermo Mass, Tokyo, Japan) with a heating rate of 293 K/min from 313 to 1573 K in a flow of 250 mL/min He gas.

HFA was synthesized using the following method. A total of 6.0 mol/L of H_3PO_4 solution and 2.0 mol/L of a HF solution were mixed and aged for 1 day in N_2 gas, which was dropped slowly into a 10.0 mol/L $Ca(OH)_2$ suspension with vigorous stirring at room temperature. The molar ratios of Ca^{2+}, PO_4^{3-}, and F^- were adjusted to be 10, 6, and 2. The resultant material was aged for 1 day, and the final pH was about 7.0. Spherical HFA powder was then fabricated using a spray dryer (Advantec DRZ350WB, Tokyo, Japan). The suspension was atomized under a pressure of 1.5 MPa at a flow rate of 500 mL/h, and the inlet and outlet temperatures of the nozzle were adjusted to 180 and 80 °C, respectively. The spray-dried powder was then heated at 1073 K for 3 h.

Fabrication of a Sintered Body. I_2-zeolite A after HA coating and a spherical HFA powder were mixed at a weight ratio of 15/85. The powder obtained was sintered using a PECS method (34−36). The sample was pressed uniaxially at 50 MPa in a vacuum of 0.6×10^{-2} Pa throughout the sintering process. The

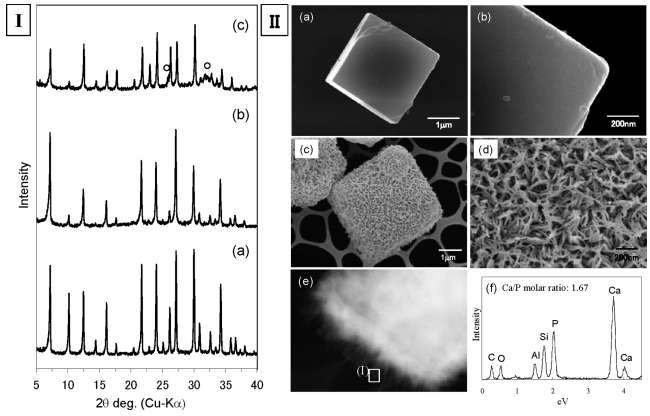

FIGURE 1. Crystal phases of Ca-zeolite A (I-a), I_2-zeolite A (I-b), and I_2-zeolite A coated with HA (I-c) by XRD (open circles; HA), the changing morphology of the zeolite surface before (II-a,b) and after (II-c,d) HA coating by SEM, and the surface observation (II-e) and element analysis (II-f) by STEM and EDX.

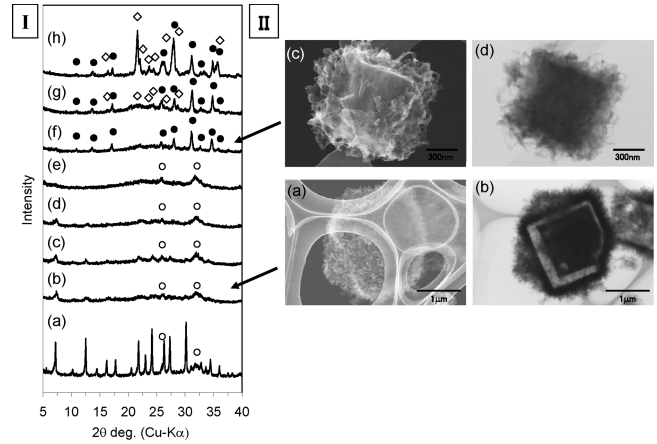

FIGURE 2. Crystal-phase changes of I_2-zeolite A coated with HA by the heating treatment at elevated temperatures [298 K (I-a), 473 K (I-b), 673 K (I-c), 873 K (I-d), 1073 K (I-e), 1223 K (I-f), 1273 K (I-g) and 1473 K (I-h): open circles, HA; black circles, TCP; open rhomboids, feldspar; the other diffractions are attributed to the zeolite A structure] by XRD and the changing morphology at 473 K (II-a,b) and 1223 K (II-c,d) by STEM.

temperature was increased to 1223 K at a rate of 323 K/min. After 1223 K was maintained for 10 min, the sample was slowly cooled to 873 K at a rate of 278 K/min and was further cooled to room temperature after the electric current was stopped and the pressure released. The density of the sintered body of 20 mm in diameter and 4 mm in thickness was measured based on Archimedes' principal. The relative density was calculated based on 85 wt % HFA (theoretical density: 3.16 g/cm^3) and 15 wt % amorphous glass (theoretical density: 2.20 g/cm^3). A boundary structure in the sintered body with the three different phases—zeolite A, HA, and HFA—was observed by STEM, and the elements present were analyzed by EDX. A specimen of 100 nm in thickness was prepared by a focused ion beam (FIB; Noran Vantage FB-2100, Hitachi, Tokyo, Japan) and pick-up method. The iodine binding energies (I3d) of the zeolite phase in the sintered body were measured by X-ray photoelectron spectroscopy (XPS; Shimazu AXIS-AS, Tokyo, Japan), and the iodine content was investigated by IC.

Iodine Elution Test. Three sintered bodies were placed in distilled water for 56 days with a solid (cm^2)/liquid (mL) mixing ratio of 1/100. The reaction was carried out under an argon atmosphere in a closed box with the oxygen concentration kept below 1 mg/L. The eluted amounts of iodine and phosphorus ions were measured by ICP-MS (Seiko SPQ9000). Silicon, magnesium, calcium, and sodium ions were measured by ICP-AES, and fluorine ions were measured by IC.

RESULTS AND DISCUSSION

Structure and Morphology of Zeolite Coated with Hydroxyaptite. Figure 1(I) shows the XRD patterns for (I-a) pure Ca-zeolite A, (I-b) I_2-zeolite A, and (I-c) I_2-zeolite A after HA coating. Iodine adsorption on zeolite A did not produce new peaks or a change in the peak positions, but it did cause a change in the intensities of the peaks at 2θ values of 10.2° and 26.2° (I-a,b). This was attributed to a reduction in the (Si,Al)—O distance in Ca-zeolite A as a result of iodine adsorption (40). The XRD intensities of I_2-zeolite A after HA coating were also changed because of the partial ion exchange of ammonium ions with calcium ions (I-c) (41, 42). The reaction yield was 46%, which was calculated under reactive conditions without iodine molecules similar to those presented in our previous report (43). Thus, I_2-zeolite has an aluminosilicate composition of $(NH_4)_{6.4}Ca_{2.8}Si_{12}Al_{12}O_{48}$ (NH_4-zeolite). In Figure 1(I-c), the two circles indicate broad diffractions attributed to the formation of the HA phase. Figure 1(II) shows SEM images of the morphology of I_2-zeolite A before and after HA coating. In both cases, cubic automorphisms (II-a,b) in addition to needlelike HA crystals of about 200 nm in length (II-c,d) are observed evenly on the surface. These HA formations are due to an ion-exchange reaction of calcium ions on Linde type A with ammonium ions in an ammonium phosphate solution, followed by a reaction between the calcium and phosphate ions on the surface of Linde type A. Thus, neither iodine adsorption nor HA coating was found to affect the morphology of zeolite A. From the selected-area EDX spectrum shown in Figure 1-(II-e,f), the Ca/P ratio of HA was calculated at 1.67, which is the same as the theoretical HA composition. In addition, crystal growth of HA was found to proceed in a similar manner on both Ca-zeolite A and I_2-zeolite A.

Thermal Stability of Iodine on the Zeolite Coated with HA. The crystal phases and morphology of I_2-zeolite A after HA coating heated at elevated temperatures were investigated using XRD and STEM, respectively, as shown in Figure 2(I),(II). Following heating at 473 K, I_2-zeolite A after HA coating exhibited a dramatic decrease in the diffraction intensity due to the appearance of an amorphous phase, and only the HA crystal phase was observed [Figure 2(I-b)]. The formation of a low-density amorphous phase was clearly observed by STEM at the interfaces between zeolite A and HA (Figure 2(II-a,b)). A heat treatment at more than 1223 K caused a change of the HA phase to tricalcium phosphate (TCP; $Ca_3(PO_4)_2$) (Figure 2(I-f)). The TCP phase appeared as a result of the nonstoichiometric composition of the HA phase. This phenomenon is known to occur by the formation of Ca-deficient HA in P-rich conditions, as is the case in this study. Although a Ca/P ratio of 1.67 was determined by EDX, the ratio for the HA structures near the zeolite A surface is probably closer to 1.50. The thermal treatment did not change the cubic morphology of zeolite A but resulted in the crystal growth of TCP on its surfaces, as shown in the STEM images (Figure 2(II-c,d)). In addition, the

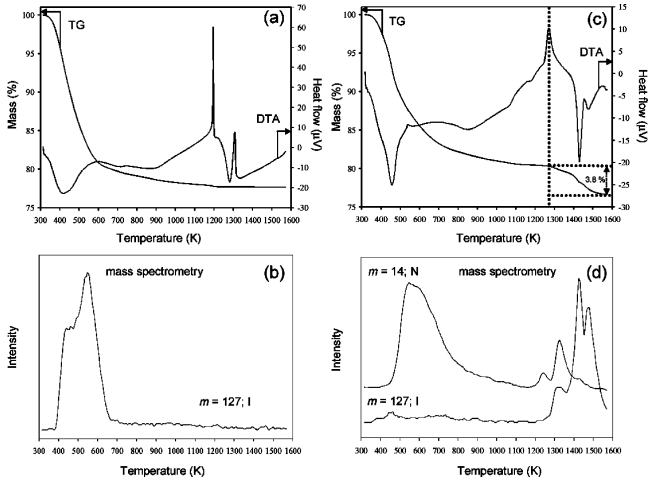

FIGURE 3. TG−DTA/MS spectra of I_2-zeolite A (a and b) and I_2-zeolite A coated with HA (c and d).

crystalline feldspar phase was formed at 1473 K (Figure 2-(I-h)). The iodine content in I_2-zeolite A without and with the HA nanolayer was measured at 3.5 and 3.3 wt %, respectively. The chemical composition without the HA nanolayer can be written as $Ca_{5.72}Na_{0.56}Si_{12}Al_{12}O_{48}(I_2)_{0.24}$. This iodine content is much lower than published adsorption values for zeolite A (40). The loss of iodine following HA coating is thought to be related to the decrease in the relative amount of zeolite A resulting from the coating. In fact, the decreased weight of iodine corresponded with that of zeolite A calculated from the HA reaction yield (43). This result implies that the iodine is effectively maintained in zeolite A after HA coating (ion-exchange reaction).

The thermal stability of iodine adsorbed into zeolite A was analyzed by a TG−DTA system equipped with a mass spectrometer. The TG−DTA curve and the mass spectra for I_2-zeolite are shown in parts a and b of Figure 3, respectively, and those for I_2-zeolite after HA coating in parts c and d of Figure 3, respectively. A decrease in the weight of I_2-zeolite A of 22.3% occurred from room temperature to 1573 K. The broad endothermic peak at 423 K was attributed to the adsorbed water in the zeolite A cavities, and the exothermic peaks at 1196 and 1309 K were due to the phase changes to the amorphous and feldspar phases (Figure 3a) (10). The elimination of iodine from the zeolite cavities was confirmed by the mass spectrum for mass number 127 from 323 to 723 K (Figure 3b). This elimination temperature is below that required for the sintering process. On the other hand, the elimination behavior of iodine molecules from I_2-zeolite A with HA coating appears to be completely different, except for the weight loss at 23.3% and the vaporization of water with an endothermic peak at 456 K. The elimination of N_2 from zeolite A was confirmed by the mass spectrum for mass number 14 (N) from 423 to 873 K and over 1223 K with two exothermic peaks at 1246 and 1326 K (Figure 3c,d). The N_2 elimination in the temperature range 423−873 K was attributed to the elimination of NH_3 from NH_4-zeolite A cavities, which occurred during formation of the amorphous phase. This phase change from NH_4-zeolite A to amorphous was also identified by XRD [Figure 1(I-b)]. The appearance of N_2 up to 1223 K is probably due to the amorphous phase on the zeolite A surface acting as an effective barrier, and the elimination of N_2 over 1496 K is due to the phase change to feldspar. From the mass spectrum for mass number 127, a weight loss of 3.8% was observed above 1253 K with two endothermic peaks at 1432 and 1482 K (Figure 3c,d). The broad exothermic peak at 1165 K appeared to be due to a complete change to the amorphous phase, and that at 1253 K is due to the phase change to feldspar (Figure 3c). Thus, the elimination of iodine occurred during crystallization. The phase change from the amorphous phase to feldspar was also observed by XRD [Figure 2(I-g,h)].

The above results can be explained by the partial blockage of the α-cage apertures by ammonium ions and a change to the amorphous phase from the zeolite crystal phase at low temperature (473 K). The apertures of α cages in the zeolite A structure are controlled by cations such as sodium, potassium, and calcium ions. The exchange sites are different, which causes a change in the α-cage, β-cage, and double 4-ring aperture sizes. In addition, the site selectivity of cations is determined by the interaction energy between lattices; sodium ions are selectively located at β-cage positions ($8Na^+$) and then at α-cage ($3Na^+$) and double 4-ring (Na^+) positions. Potassium ions are selectively located at α-cage positions. Calcium ions are selectively located only at β-cage positions ($4Ca^{2+}$) (10). This means that when sodium and potassium ions in each cage are exchanged with calcium ions, the α-cage positions become vacant [the distance of O(1)−O(1) is 0.42 nm] and have apertures larger than the diameter of 0.40 nm for the iodine molecule. Thus, zeolite A has adjustable α-cage apertures, which are controlled by countercations, and the apertures can be used as barriers to prevent the elimination of iodine molecules. In this case, I_2-zeolite A (Ca-type) has only iodine molecules in the α cages, and the aperture sizes are 0.42 nm. Furthermore, the zeolite A structure was maintained up to a temperature of 1073 K. Therefore, the elimination of 0.40-nm-diameter iodine molecules was easily achieved by heating from 323 to 723 K. On the other hand, I_2-zeolite A (NH_4-type) after HA coating has both iodine molecules and ammonium ions in the α cages. The apertures are about 0.30 nm, which is smaller than the I_2 molecules. The iodine molecules are maintained in the structure at room temperature because of the partial blockage of the apertures by ammonium ions located in the α cages. Furthermore, the pore structures on the surface of NH_4-zeolite A are gradually transformed from the cubic structure of zeolite A to an amorphous phase at 473 K.

Thus, the presence of ammonium ions in the α cages and the formation of the amorphous phase at low temperature both play an important role as barriers that prevent the elimination of iodine molecules at temperatures up to 1253 K.

Iodine in a Three-Component Sintered Body. A three-component sintered body of I_2-zeolite A, HA nanolayer, and HFA was successfully fabricated at 1223 K by the

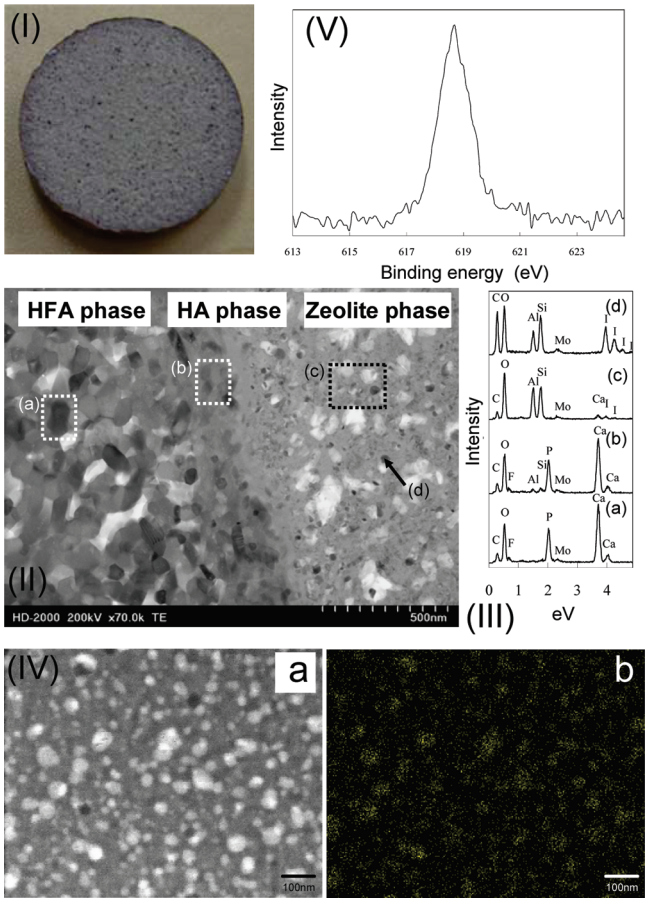

FIGURE 4. Observation of a three-component boundary and the states of iodine in a sintered body. Photograph (I), STEM image (II), the EDX spectra (III-a,b,c) in part II, STEM image (IV-a), and EDX mapping (iodine L-line) of the zeolite phase in the sintered body (IV-a) and the XPS $I3d_{5/2}$ spectrum of the zeolite phase in the sintered body (V).

PECS method and had a relative density of up to 98.1 ± 2.2 %, taking into account the HFA/zeolite weight ratio. The sintered body was brown in color because of the retained iodine [Figure 4(I)]. In contrast to the results previously reported (44), no breaking or cracking was found to occur during the sintering process because of the existence of the HA nanolayer. An STEM image of a boundary region between the three components is shown in Figure 4(II). The grain size in the HFA matrix was smaller than 300 nm, which is typical in the PECS method to obtain high sinterability (35, 36). EDX analysis of the HFA matrix showed that no silicon or aluminum was present [Figure 4(III-a)]. A unique nanolayer structure at the interface between the HFA matrix and I_2-zeolite was clearly observed and chemical analysis at this region indicated the presence of small amounts of silicon and alumina [Figure 4(III-b)]. It can be concluded that the HA nanolayer plays an important role in improving the interaction between I_2-zeolite A and the HFA matrix. Electron diffraction patterns could not be obtained from the zeolite A region because it had an amorphous phase. Chemical elements attributed to zeolite A, such as silicon and alumina, were clearly detected by EDX, as shown in Figure 4(III-c). Iodine was also clearly detected from the regions of dark contrast seen in Figure 4(II and III-c,d). Figure 4(IV) shows an elemental mapping for iodine, which is found to be confined to regions approximately 30 nm in size. The distribution of iodine in the amorphous zeolite A was homogeneous, and it was not detected from regions other than zeolite A. To confirm the chemical state of iodine in zeolite A, the XPS spectrum was examined. The $I3d_{5/2}$ spectrum of the zeolite A phase is shown in Figure 4(V). The binding energy attributed to $I3d_{5/2}$ was observed at 618.7 eV, which could be fitted to one symmetrical line and agreed with the published value for iodides (45).

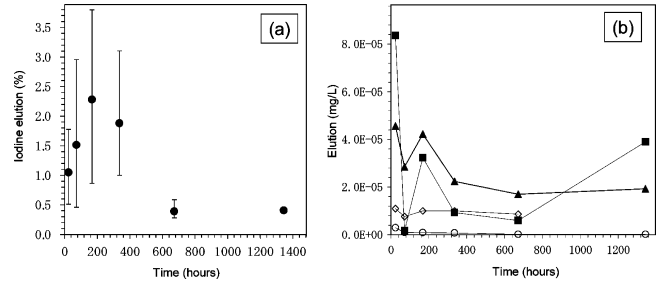

FIGURE 5. Elution of iodine ions (a) and other ions (b) from the sintered body in distilled water: black circles, I; black squares, Si; black triangles, Ca; open squares, P; open circles, F.

The iodine content in the sintered body (I_2-zeolite A after HA coating with a HFA weight ratio of 85:15) was 0.51 ± 0.03 wt %, indicating that more than 99% at the iodine was retained. When a sintering temperature of 1273 K was used, the iodine content was found to decrease to 67%. Furthermore, in the case of an I_2-zeolite without an apatite coating in the two-component (I_2-zeolite A and HFA) sintering process, the iodine was not retained on heating. The elution of an iodine ion and other ions from the sintered body was investigated in distilled water under an argon gas atmosphere. The results are shown in Figure 5. After soaking for 162 h, 4.9 wt % of the iodine was eluted from I_2-zeolite A. The elution was found to occur in the near surface layer to a depth of 800 μm, determined from the homogeneous distribution of I_2-zeolite A. The eluted amount decreased to 0.4 wt % after 672 h and remained unchanged up to 1334 h (Figure 5a). A similar elution of calcium and silicon ions was observed, but fluorine and phosphorus ions were found to elute more slowly. The elution of aluminum and sodium ions was below the detection limits (Al, 3.7×10^{-7} M; Na, 8.7×10^{-8} M). Thus, the iodine ion was eluted from the amorphous phase containing calcium and silicon ions, which indicates that iodine elution depended on the mixing of states of zeolite A covered with HA and HFA before the PECS sintering. This means that this elution can be prevented by mixing methods, such as the construction of a HFA wall at the outer layer.

CONCLUSIONS

We have reported on the fabrication of a compound sintered body of iodine-adsorbed zeolite A, HA, and HFA as a long-term encapsulation material for radioactive iodine-129. The outer phase was highly crystalline HFA in which the HA nanolayer plays an important role for successful sintering. The elution of iodine molecules in low-dioxygen

water, similar to that found within the Earth's crust, was found to occur only in the surface layer of the sintered body. This three-phase ceramic composite is a promising alternative to the common vitrification process.

Acknowledgment. This work was supported by special coordination funds from the Ministry of Education, Culture, Sports, Science and Technology of the Japanese Government and by a Grant-in-Aid for Scientific Research (21760541) from the Japan Society for the Promotion of Science. The authors are indebted to Dr. H. Nishimura, National Institute for Materials Science, for his kind assistance with PECS.

REFERENCES AND NOTES

(1) (a) Suvorova, V. A.; Akhmedzhanova, G. M.; Kotelnikov, A. R. *Radiochemistry* **1997**, *39*, 359–369. (b) Suvorova, V. A.; Zyryanov, V. A.; Kotelnikov, A. R. *Eng. Geol. Environ., Proc. Int. Symp.* **1997**, *1–3*, 2199–2202.
(2) Ojovan, M. I.; Lee, W. E. *An Introduction to Nuclear Waste Immobilisation*; Elsevier Science: Amsterdam, The Netherlands, 2005.
(3) Sazarashi, M.; Takeshita, K.; Kumagai, M.; Takashima, Y.; Komatsu, H.; Inami, S. *J. At. Energy Soc. Jpn.* **1993**, *35*, 1095–1096.
(4) (a) Takeshita, K.; Tashima, Y.; Matsumoto, S.; Inami, S. *J. Nucl. Sci. Technol.* **1995**, *32*, 941–943. (b) Takeshita, K.; Matsumoto, S.; Kumagai, M.; Koga, J.; Takashima, Y. *J. At. Energy Soc. Jpn.* **1992**, *34*, 1161–1165.
(5) Funabashi, K.; Fukasawa, T.; Kikuchi, M. *Nucl. Technol.* **1995**, *108*, 266–372.
(6) Balsley, S. D.; Brady, P. D.; Krumhansl, J. L.; Anderson, H. L. *J. Soil Contamin.* **1998**, *2*, 125–141.
(7) Nilchi, A.; Khanchi, A.; Maragheh, M. G. *Talanta* **2002**, *56*, 383–393.
(8) Riebe, B.; Dultz, S.; Bunnenberg, C. *Appl. Clay Sci.* **2005**, *28*, 9–16.
(9) Dyer, A. *An introduction to zeolite molecular sieves*; John Wiley & Sons, Inc.: New York, 1988.
(10) Breck, D. W. *Zeolite Molecular Sieves, Chemistry and Uses*; John Wiley & Sons, Inc.: New York, 1991.
(11) Watanabe, Y.; Yamada, H.; Tanaka, J.; Komatsu, Y.; Moriyoshi, Y. *Sep. Sci. Technol.* **2004**, *39*, 2091–2104.
(12) Colyer, L. M.; Greaves, G. N.; Dent, A. J.; Fox, K. K.; Carr, S. W.; Jones, R. H. *Nucl. Instrum. Methods Phys. Res.* **1995**, *B97*, 107–110.
(13) Juoi, J. M.; Ojovan, M. I.; Lee, W. E. *J. Nucl. Mater.* **2008**, *372*, 358–366.
(14) Basch, A.; Hartl, M.; Behrens, P. *Microporous Mesoporous Mater.* **2007**, *99*, 244–250.
(15) Bronic, J.; Sekovanic, L.; Muzic, A.; Biljan, T.; Kontrec, J.; Subotic, B. *Acta Chim. Slov.* **2006**, *53*, 166–171.
(16) Matsuoka, S.; Nakamura, H.; Takaaki, T. *J. Nucl. Sci. Technol.* **1984**, *21*, 862–870.
(17) Rehakova, M.; Cuvanova, S.; Wadsten, T.; Saly, V.; Nagyova, S. *Solid State Ionics* **1993**, *66*, 189–194.
(18) Deb, S. K.; Wilding, M.; Somayazulu, M.; McMillan, P. F. *Nature* **2001**, *414*, 528–530.
(19) Greaves, G. N.; Meneau, F.; Sapelkin, A.; Colyer, L. M.; Gwynn, I. A.; Wade, S.; Sankar, G. *Nat. Mater.* **2003**, *2*, 622–629.
(20) Navrotsky, A. *Nat. Mater.* **2003**, *2*, 571–572.
(21) Yamada, H.; Yokoyama, S.; Watanabe, Y.; Uno, H.; Tamura, K. *Sci. Technol. Adv. Mater.* **2005**, *6*, 394–398.
(22) Barrer, B. M. *Zeolite: Science and Technology*; Martinus Nijhoh Publishers: Dordrecht, The Netherlands, 1984.
(23) Gross, K. A.; Rodriguez-Lorenzo, L. M. *Biomaterials* **2004**, *25*, 1375–1384.
(24) Gross, K. A.; Rodriguez-Lorenzo, L. M. *Biomaterials* **2004**, *25*, 1385–1394.
(25) Gross, K. A.; Bhadang, K. A. *Biomaterials* **2004**, *25*, 1395–1405.
(26) Barinov, S. M.; Rustichelli, F.; Orlovskii, V. P.; Lodini, A.; Oscarsson, S.; Firstov, S. A.; Tumanov, S. V.; Millet, P.; Rosengren, A. *J. Mater. Sci.: Mater. Med.* **2004**, *15*, 291–296.
(27) Chen, Y. M.; Miao, X. G. *Biomaterials* **2005**, *25*, 1205–1210.
(28) Senamaud, N.; Bernache-Assollant, D.; Champion, E.; Heughebaert, M.; Rey, C. *Solid State Ionics* **2004**, *15*, 291–296.
(29) Rodriguez-Lorenzo, L. M.; Hart, L. M.; Gross, K. A. *Biomaterials* **2003**, *24*, 3777–3785.
(30) Moreno, E. C.; Kresak, M.; Zaharadnik, R. T. *Nature* **1974**, *247*, 64–65.
(31) Akao, M.; Aoki, H.; Kato, K. *J. Mater. Sci.* **1981**, *16*, 908–812.
(32) Ikoma, T.; Yamazaki, A.; Nakamura, S.; Akao, M. *J. Mater. Sci. Lett.* **1999**, *18*, 1225–1228.
(33) Takikawa, K.; Akao, M. *J. Mater. Soc.: Mater. Med.* **1996**, *7*, 439–445.
(34) Watanabe, Y.; Ikoma, T.; Monkawa, A.; Suetsugu, Y.; Yamada, H.; Tanaka, J.; Moriyoshi, Y. *J. Am. Ceram. Soc.* **2005**, *88*, 243–245.
(35) Gu, Y. W.; Loh, N. H.; Khor, K. A.; Tor, S. B.; Cheang, P. *Biomaterials* **2002**, *23*, 37–43.
(36) Nakahira, A.; Tamai, M.; Aritani, H.; Nakamura, S.; Yamashita, K. *J. Biomed. Mater. Res.* **2002**, *62*, 550–557.
(37) BenAyed, F.; Bouaziz, J.; Bouzouita, K. *J. Eur. Ceram. Soc.* **2000**, *20*, 1069–1076.
(38) BenAyed, F.; Bouaziz, J.; Bouzouita, K. *J. Alloys Compd.* **2001**, *322*, 238–245.
(39) Watanabe, Y.; Ikoma, T.; Suetsugu, Y.; Yamada, H.; Tamura, K.; Komatsu, Y.; Tanaka, J.; Moriyoshi, Y. *J. Eur. Ceram. Soc.* **2006**, *26*, 481–486.
(40) Karl, S.; Davidm, P. S. *Acta Crystallogr.* **1967**, *22*, 162–170.
(41) Watanabe, Y.; Ikoma, T.; Suetsugu, Y.; Yamada, H.; Tamura, K.; Komatsu, Y.; Tanaka, J.; Moriyoshi, Y. *J. Eur. Ceram. Soc.* **2006**, *26*, 469–474.
(42) Matsumoto, T.; Goto, Y.; Urabe, K. *J. Ceram. Soc. Jpn.* **1995**, *103*, 93–95.
(43) Watanabe, Y.; Moriyoshi, Y.; Suetsugu, Y.; Ikoma, T.; Kasama, T.; Hashimoto, T.; Yamada, H.; Tanaka, J. *J. Am. Ceram. Soc.* **2004**, *87*, 1395–1397.
(44) Yamada, H.; Watanabe, Y.; Tamura, K. *Nukleonika* **2006**, *51*, 61–67.
(45) Rehakova, M.; Sopkova, A.; Casciola, M.; Bastl, Z. *Solid State Ionics* **1993**, *66*, 189–194.

AM900251M